

Journal of Biomedical Optics

SPIEDigitalLibrary.org/jbo

Simultaneous characterization of pancreatic stellate cells and other pancreatic components within three- dimensional tissue environment during chronic pancreatitis

Wenyan Hu
Ling Fu

Simultaneous characterization of pancreatic stellate cells and other pancreatic components within three-dimensional tissue environment during chronic pancreatitis

Wenyan Hu^{a,b} and Ling Fu^{a,b}

^aHuazhong University of Science and Technology, Britton Chance Center for Biomedical Photonics, Wuhan National Laboratory for Optoelectronics, Wuhan 430074, China

^bHuazhong University of Science and Technology, Department of Biomedical Engineering, MoE Key Laboratory for Biomedical Photonics, Wuhan 430074, China

Abstract. Pancreatic stellate cells (PSCs) and other pancreatic components that play a critical role in exocrine pancreatic diseases are generally identified separately by conventional studies, which provide indirect links between these components. Here, nonlinear optical microscopy was evaluated for simultaneous characterization of these components within a three-dimensional (3-D) tissue environment, primarily based on multichannel detection of intrinsic optical emissions and cell morphology. Fresh rat pancreatic tissues harvested at 1 day, 7 days, and 28 days after induction of chronic pancreatitis were imaged, respectively. PSCs, inflammatory cells, blood vessels, and collagen fibers were identified simultaneously. The PSCs at day 1 of chronic pancreatitis showed significant enlargement compared with those in normal pancreas ($p < 0.001$, analysis of variance linear contrast; $n = 8$ for each group). Pathological events relating to these components were observed, including presence of inflammatory cells, deposited collagen, and phenotype conversion of PSCs. We demonstrate that label-free nonlinear optical microscopy is an efficient tool for dissecting PSCs and other pancreatic components coincidentally within 3-D pancreatic tissues. It is a prospect for intravital observation of dynamic events under natural physiological conditions, and might help uncover the key mechanisms of exocrine pancreatic diseases, leading to more effective treatments.

© The Authors. Published by SPIE under a Creative Commons Attribution 3.0 Unported License. Distribution or reproduction of this work in whole or in part requires full attribution of the original publication, including its DOI. [DOI: [10.1117/1.JBO.18.5.056002](https://doi.org/10.1117/1.JBO.18.5.056002)]

Keywords: nonlinear optical microscopy; chronic pancreatitis; pancreatic stellate cells; collagen fibers; inflammatory cells; microvessel.

Paper 12769R received Dec. 3, 2012; revised manuscript received Feb. 26, 2013; accepted for publication Mar. 20, 2013; published online May 2, 2013.

1 Introduction

Pancreatic stellate cells (PSCs) are fat-storing cells resident in periacinar space of exocrine pancreas. They transform to an activated state in response to pancreatic injury or inflammation.^{1,2} Activated PSCs serve as key participants in the pathobiology of major disorders of the exocrine pancreas, including chronic pancreatitis and pancreatic cancer.¹ Other pancreatic components such as inflammatory cells, blood vessels, and extracellular matrix also play important role in the exocrine pancreatic diseases.³⁻⁵ These components are reported to interact with each other and lead to the progression of these diseases conjointly. For example, PSCs respond to inflammatory cytokines,² and activated PSCs contribute to the recruitment of inflammatory cells to the inflamed pancreas.⁶ PSCs constitutively produce vascular endothelial growth factor, and they might be responsible for angiogenesis.⁷ Abundant activated PSCs are also found to be present in pancreatic fibrotic areas,⁸⁻¹⁰ and accumulated data have proven that sustained activation of PSCs is the main mediator of fibrogenesis associated with pancreatitis.^{11,12} Detailed elucidation of the progressive cascade of the above pathogenic

processes should help unravel early and central event in these diseases and promote the development of improved therapeutic strategies.

Considerable progress has been made in understanding the pathogenesis of the exocrine pancreatic diseases, especially after the first isolation and characterization of PSCs in the pancreas.¹³ Our current knowledge about the pathophysiologic processes stems largely from investigations based on pancreatic cell culture and tissue sections. Unfortunately, cell cultures do not necessarily reconstitute their characteristics within three-dimensional (3-D) tissue organization, where they are surrounded by other cell types and exposed to a multiplicity of factors, and one of the major dilemmas is the fact that they undergo transformation to an activated phenotype after isolation during *in vitro* culture.^{14,15} Studies of tissue sections have the capability to provide information with relatively preserved tissue structure at a specific slice plane. However, they are limited by coregistration between slices for appreciation of 3-D structures,¹⁶ as well as the distortions and artifacts caused by microtome slicing.¹⁷ Besides, assays for the identification of individual pancreatic components are generally performed separately at different slice planes. For example, immunostaining for at least two markers such as desmin and α smooth muscle actin (α -SMA) are performed to detect the activated PSCs.^{6,14} Additional staining of serial sections for the other tissue components is required to investigate the relationships between PSCs and those

Address all correspondence to: Ling Fu, Huazhong University of Science and Technology, Britton Chance Center for Biomedical Photonics, Wuhan National Laboratory for Optoelectronics, Wuhan 430074, China. Tel: (86) 27-87792033; Fax: (86) 27-87792034; E-mail: lfu@mail.hust.edu.cn

components. Therefore, the traditional research methods fail to visualize the distribution of multiple components within 3-D tissue structure at the same time, and thus, it is difficult to observe the direct interactions between different components involved in pancreatic pathogenesis. Simultaneous characterization of multiple components within 3-D tissue environment would allow precise dissecting of the relationships between PSCs and other pancreatic components and provide new insights into the understanding of the pathogenic processes during exocrine pancreatic diseases.

During the past two decades, nonlinear optical microscopy has emerged as a new means for 3-D imaging of thick tissues in real time and at subcellular resolution, using both two-photon excited fluorescence (TPEF) and second harmonic generation (SHG) signals.^{18,19} Most importantly, nonlinear optical imaging allows simultaneous excitation of multiple endogenous optical biomarkers by a single wavelength excitation.^{20,21} Consequently, different biochemical constituents of cellular or extracellular origins with various emission wavelengths can be detected through multiple channels, which enables simultaneous identification of different tissue components.^{16,22,23} Using this method, stromal collagen, which is the major source of SHG signals in extracellular matrix, has been recognized from cellular components.^{24–26} Lymphatic cells have been distinguished from the other gastric tissue types due to a broad emission that possibly originates from phospholipids, known to be a significant component of lymphocytes.¹⁶ Besides, morphological characteristics obtained by nonlinear optical microscopy can also provide information relating to the differentiation of multiple cell types. Macrophages, fibroblasts, and lymphocytes have been isolated by the cell shapes revealed by intrinsic fluorescence.²² As a result, based on the intrinsic optical features including emission spectrum and morphological signatures, nonlinear optical microscopy has potential for the simultaneous inspection of multiple components in pathological tissues.

Label-free imaging of pancreatic tissues by TPEF microscopy was first used to reveal the metabolic mechanisms of endocrine pancreatic islets.^{27,28} Our previous work on exocrine pancreatic tissues using nonlinear optical microscopy has been reported, demonstrating that the acinar cells and extracellular matrix in fresh pancreatic tissues can be visualized by intrinsic TPEF signals from nicotinamide adenine dinucleotide (NADH) and flavin adenine dinucleotide (FAD) and SHG signals from collagen fibers, respectively.²⁹ This work did not manage to recognize sparse PSCs from dense acinar cells in tissue environment, though PSCs show long cytoplasmic processes compared with pyramidal acinar cells.¹ A recent study has reported Ca²⁺ signaling events in PSCs stained with fluorescent calcium indicators, and the intrinsic fluorescence from cellular vitamin A in PSCs was also detected to show the morphology of PSCs in pancreatic tissues.³⁰ At present, there has been no report on synchronous characterization of PSCs and other pancreatic components including inflammatory cells, blood vessels, and the extracellular matrix within 3-D pancreatic acini using intrinsic optical emissions. Taking advantage of multichannel, two-photon imaging and information of cell morphology, nonlinear optical microscopy might allow simultaneous characterization of multiple pancreatic components during pancreatic disease progression.

In this study, our aim is to investigate whether the pancreatic components involved in pancreatic diseases can be simultaneously delineated within 3-D tissue environment by intrinsic

optical emissions and cell morphology and what detailed pathological processes during chronic pancreatitis can be achieved.

2 Materials and Methods

2.1 Animal Model and Preparation of Specimens

All the experiments followed procedures approved by the Institutional Animal Ethics Committee of Huazhong University of Science and Technology.

Male Sprague-Dawley rats weighing 120 to 150 g were purchased from the Animal Biosafety Level III Laboratory (Wuhan, China) and housed under specific pathogen-free conditions. The experimental model of chronic pancreatitis was induced by a single intravenous administration of dibutyltin dichloride (DBTC), as described elsewhere.³¹ Briefly, DBTC (Sigma-Aldrich, China) was first dissolved in 100% ethanol (two parts) and mixed with glycerol (three parts), then the DBTC solution was injected into the tail vein at a dose of 8 mg/kg body weight.

At 1, 7, and 28 days after the application of the DBTC, animals were sacrificed with an overdose of isoflurane. The fresh pancreatic specimens were excised and immediately imaged in phosphate buffered saline (PBS) within 1 h after dissection. A part of each pancreas was used for histological analysis [haematoxylin-eosin (H&E) staining, Masson's trichrome staining, and immunostaining for desmin and α -SMA]. The images of the three groups of inflammatory tissues were compared with those of the normal group. Ten rats were used for the normal group and eight rats per group were used for all the pancreatitis groups.

2.2 Nonlinear Optical Imaging and Spectral Measurements

Nonlinear optical imaging was performed using a modified system based on a commercial microscope (Fluoview 1000, Olympus, Japan), as described previously.²⁹ It is reported that the two-photon absorption of the major intrinsic fluorophores such as NADH and FAD decreases as the excitation wavelength increases in the range of 700 to 900 nm.²¹ We tuned the excitation wavelength in the 730 to 890 nm range and found that 750 nm was the optimal wavelength to give the best signal-to-noise ratio in our microscopic system. A tunable Ti:Sapphire laser (Mai Tai, Spectra-Physics) operating at 750 nm was used for excitation, except where otherwise noted. A water-immersion objective (60 \times /1.2 NA water-immersion, Olympus) was employed for focusing the excitation beam into tissue samples and collecting the backscattered intrinsic nonlinear optical signals. The average laser power on the surface of the sample was about 15 mW. The scanning rate was 10 μ s/pixel. The emission signals are detected by three channels in the nondescanned mode. A narrow bandpass filter (FF01-380/14-25, Semrock) was used for the detection of SHG signals (380 \pm 7 nm; blue). Another two emission filters (FF01-445/45-25 and FF01-530/43-25; Semrock) were used to extract the intrinsic TPEF signals for the differentiation of acini, PSCs, and other nonacinar cells. The TPEF signals were detected with the same system parameters, including the voltage, gain, and offset of the photomultiplier tubes. The nonlinear optical signals were presented by the pseudocolor images. Blue, green, and red color-coded images correspond

to SHG signals, TPEF signals between 423 and 467 nm, and TPEF signals between 509 and 551 nm, respectively.

For the spectral measurements, the emitted signals are collected by a fiber bundle with a lens (focal length = 50 mm) after the dichroic mirror (FF665-Di02-25 × 36, Semrock) and sent to a spectrograph (Acton SP2356, Princeton Instruments) with a grating of 300 grooves blazed at 500 nm, followed by a thermoelectrically cooled charge-coupled device camera (PIXIS:256E, Princeton Instruments).

2.3 Quantitative Analysis of PSC Size and Collagen

To calculate the size of PSCs, the nonlinear optical image among the axial consecutive stack (z step of 1 μm) that shows the largest PSC size in appearance was chosen, and at least five images of different areas were used for each sample. The superimposed images of two TPEF channels were first processed with Adobe Photoshop CS4 (Adobe Systems Inc.) to improve contrast and dissect out the PSCs visually. The size of PSCs was evaluated by the number of pixels that each PSC accounted for and converted to area unit (μm^2) according to the size of the image. The average sizes were calculated for the normal group and pancreatitis groups harvested at different stages.

The content of collagen fibers for each specimen was evaluated by the proportion of the number of pixels that collagen fibers account for to the total number of pixels of the image. Because of the fibrous connective tissue capsule distributed in the surface of pancreas,²⁹ the SHG images of the parenchyma at an imaging depth showing the best visualization of acinar morphology were picked out for the analysis of collagen density for all samples. The SHG images were preprocessed using the MATLAB (The MathWorks) function “imadjust” for gray level adjustment to increase the contrast of the image, so that the intensities of the SHG signal acquired for different samples are comparable. The background noise is subtracted by counting the pixels with a value above the threshold of 20% of the maximal value for each image as described elsewhere.³² At least five imaging areas were calculated to get the average content value for each tissue.

Statistical significance was calculated with analysis of variance (ANOVA) linear contrast using SPSS software (SPSS). All p -values of 0.05 or less were considered to be statistically significant.

2.4 Histological Analysis

The pancreatic tissues were fixed with 10% neutral buffered formalin, and paraffin-embedded sections with a thickness of 5 μm were routinely prepared. The pancreatic tissue sections were subsequently de-waxed and rehydrated before H&E staining and Masson's trichrome staining, which were used for the detection of collagen fibers.

The phenotype of PSCs in the time course of chronic pancreatitis induced by DBTC was characterized using immunohistochemical detection of desmin and α -SMA using published techniques.¹³ Antigen retrieval was achieved by microwave heating of the tissue sections for 15 to 20 min. Endogenous peroxidase activity was blocked with hydrogen peroxide (10 min) and rinsed in PBS three times. Sections were then incubated overnight at 4°C with primary antibody [monoclonal mouse anti-desmin antibody 1/100 (ab8470) or monoclonal mouse anti- α -SMA antibody 1/200 (ab18147); Abcam, Cambridge, Massachusetts]. After three washes in PBS for 3 min each,

the ultrasensitive streptavidin-peroxidase kit (KIT-9710; Maixin Inc., Fuzhou, China) and diaminobenzidine (DAB) kit (DAB-0031; Maixin Inc., Fuzhou, China) were used for color development according to the manufacturer's instructions. Counterstaining was performed with Mayer's hematoxylin.

Histological images were acquired using an optical microscope (IX81, Olympus, Japan) equipped with a 20× air objective and a color digital industrial camera (DFK 41BU02, The Imaging Source Europe GmbH, Germany).

3 Results

3.1 Identification of PSCs in a Normal Pancreas

It can be observed from the nonlinear optical images that a small amount of collagen fibers [arrow in Fig. 1(a)] distributed around the acini composed of acinar cells [asterisks in Fig. 1(b)], which has been reported previously.²⁹ The fluorescence intensity of acinar cells detected in the red channel [Fig. 1(c)] is much lower than that in the green channel [Fig. 1(b)], indicating that the intrinsic fluorescence primarily comes from NADH with a fluorescence peak at 460 nm.²¹ The emission spectrum of acinar cells excited at 750 nm [Fig. 1(e)] extends over a wide range of wavelengths similar with NADH and FAD, which are the major cellular sources of intrinsic fluorescence. The spectrum with excitation wavelength of 820 nm, where the absorption of NADH is negligible, displays a prominent peak at about 530 nm [Fig. 1(e)], which is the characteristic of FAD.²¹ These results demonstrate that the major intrinsic fluorophore detected in the range of 445 ± 22 nm and 530 ± 21 nm in acinar cells is NADH, and FAD has a minor contribution to the autofluorescence when excited at 750 nm. Besides, the emission from collagen fibers peaks at 375 nm, verifying that the collagen fibers can be identified by SHG signals detected in the blue channel [380 ± 7 nm, arrow in Fig. 1(a)].

Specially, a few cells in the peri-acinar space with a star-like appearance and cellular processes [dotted lines in Fig. 1(c)] show higher intensity of TPEF signals in the red channel [arrowheads in Fig. 1(c)], leading to an orange color in the superimposed image of three channels [Fig. 1(d)]. The corresponding spectroscopic data exhibit a major peak around 500 nm [Fig. 1(e)], which is close to that of vitamin A.²¹ These cells are identified as PSCs according to their long cytoplasmic processes encircling the base of pancreatic acini and the presence of retinol-containing fat droplets.

Correspondingly, the anatomical structures of the pancreatic acini and collagen fibers are correspondent with H&E and Masson's trichrome staining [Fig. 2(a) and 2(b)], respectively. The immunostaining images for the expression of the intermediate filament desmin [Fig. 2(c)] show the same characteristics of PSCs with the nonlinear optical images, including the cytoplasmic processes and peri-acinar distribution. The activation marker α -SMA that only expressed around blood vessels and pancreatic ducts [Fig. 2(d)] further validated the quiescent phenotype of PSCs with vitamin A storage in normal pancreas.

The above results reveal that intrinsic emission contributions from different biochemical constitutions can be distinguished by the green (445 ± 22 nm) and red (530 ± 21 nm) channels, and combined with morphological characteristics to recognize PSCs from acinar cells in pancreatic tissues, indicating the potential to depict the other pancreatic components by nonlinear optical microscopy.

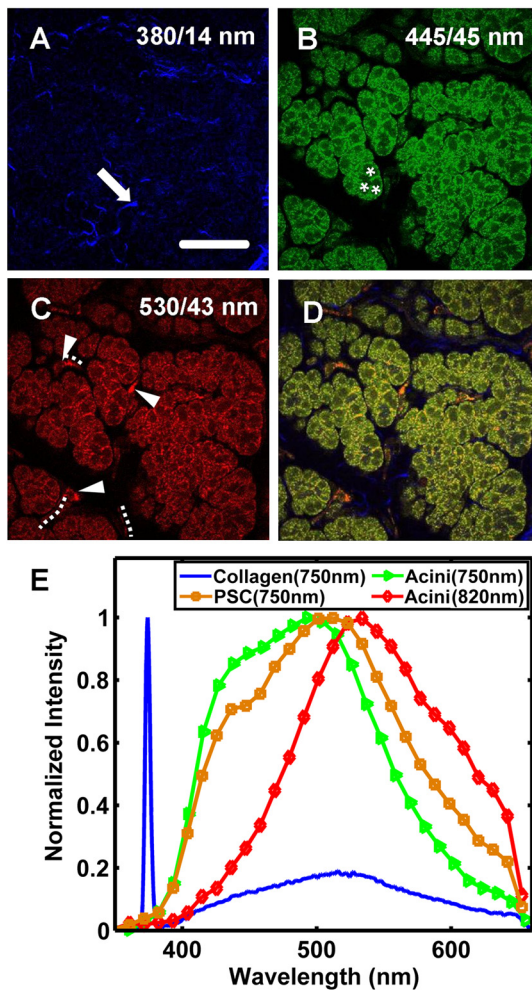


Fig. 1 Identification of pancreatic stellate cells (PSCs) in normal pancreatic tissues. The intrinsic nonlinear optical images including (a) second harmonic generation (SHG) image, (b) two-photon excited fluorescence (TPEF) image detected in the range of 423 to 467 nm, (c) TPEF image detected in the range of 509 to 551 nm, and (d) the superimposed image of the above three channels show collagen fibers and PSCs distributed around the exocrine acini. The contrast of the SHG image (a) is enhanced for better visualization using Fluoview FV10-ASW software (Version 1.4a; Olympus, Japan). The solid arrows, asterisks, solid arrowheads, and dotted lines indicate the collagen fibers, acinar cells, the PSCs, and the cellular processes of the PSCs, respectively. (e) The emission spectrum of different pancreatic components excited at 750 or 820 nm can be related with the major endogenous biochemical constituents such as collagen fibers, nicotinamide adenine dinucleotide (NADH), flavin adenine dinucleotide (FAD), and retinol. The rapid decrease of the spectra in the range of 665 nm is due to the cut-off of the dichroic mirror before the spectrograph. Scale bar is 60 μm .

3.2 Visualization of Multiple Pancreatic Components During Chronic Pancreatitis

At day 1 after the induction of chronic pancreatitis, there are no obvious alterations of the acinar structure in the nonlinear optical image [Fig. 3(a)], which is consistent with the H&E-stained image [Fig. 3(a)]. Inflammatory cells without any processes of the cytoplasm appear in the interstitium matrix at day 7 [open arrows in Fig. 3(b)]. The infiltrating inflammatory cells manifest an orange color, with high fluorescence intensity at longer wavelength (530 ± 21 nm).¹⁶ Most of these cells show parallels with the characteristics of lymphocytes including a small round or oval shape and a thin rim of cytoplasm surrounding the dark

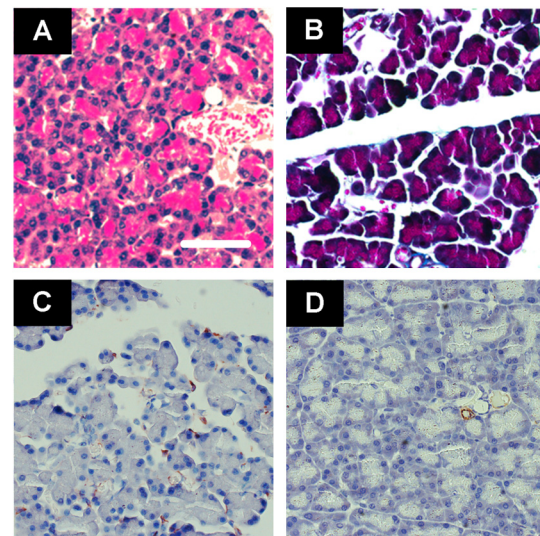


Fig. 2 Histological images of normal pancreas. (a) Haematoxylin-eosin (H&E) staining and (b) Masson's trichrome staining show the same pattern of exocrine pancreas with the nonlinear optical images (Fig. 1). (c) Desmin-positive and (d) α -SMA-negative assessed by immunostaining show that the PSCs in normal pancreas exhibit a quiescent phenotype. The morphology of PSCs revealed by immunostaining is identical to that in the nonlinear optical images (Fig. 1). Scale bar is 60 μm .

round nucleus,²² as can be found in the H&E-stained images [Fig. 3(b)]. At day 28 after the induction of chronic pancreatitis, a decrease in the number of acinar cells and the presence of tubular complexes consisting of duct-like structures with a large lumen lined by a monolayer of low cuboidal or flattened cells [asterisks in Fig. 3(c)] can be seen, which is verified by H&E staining [Fig. 3(c)]. In addition, macrophage [open arrowhead in Fig. 3(c)] with cytoplasmic inclusions²² can also be observed except for lymphocytes [open arrows in Fig. 3(c)], and they possibly play a role in the removal of necrotic cellular debris in the pancreas.

The collagen fibers in pancreatic tissues are visualized simultaneously and the density of collagen fibers during chronic pancreatitis is analyzed. As can be seen from the SHG signals, the inflamed pancreatic tissues harvested at day 7 after the induction of chronic pancreatitis show slight increase of collagen fibers around individual acini [Fig. 3(b)], while those harvested at day 28 after the induction of chronic pancreatitis develop intensive periacinar fibrosis [Fig. 3(c)]. Quantitative analysis shows that the density of collagen fibers on day 28 after the induction of chronic pancreatitis is significantly larger than the day 1 group and the normal group [Fig. 4(a); $p < 0.001$, ANOVA linear contrast; $n = 8$ for each group], which is further validated by Masson's trichrome staining [Fig. 4(b)–4(d)]. The gradual accumulation of stromal collagen fibers after the phenotype conversions of PSCs implies the contribution of activated PSCs to fibrosis in chronic pancreatitis.

Dark duct-like structure with a diameter of 6 to 9 μm is delineated at day 28 (dotted lines in Fig. 5). This structure represents blood vessels since the intrinsic fluorescence can be quenched by the heme moieties of hemoglobin in erythrocytes that exist in blood plasma. The edge of the duct is lined by thin fluorescent dots, which are resulted from a layer of flattened epithelium cells (open arrows in Fig. 5), and the spindle-shaped cell that locates adjacent to the duct (solid arrow in Fig. 5) is identical to the pericyte of a capillary vessel around base membrane of

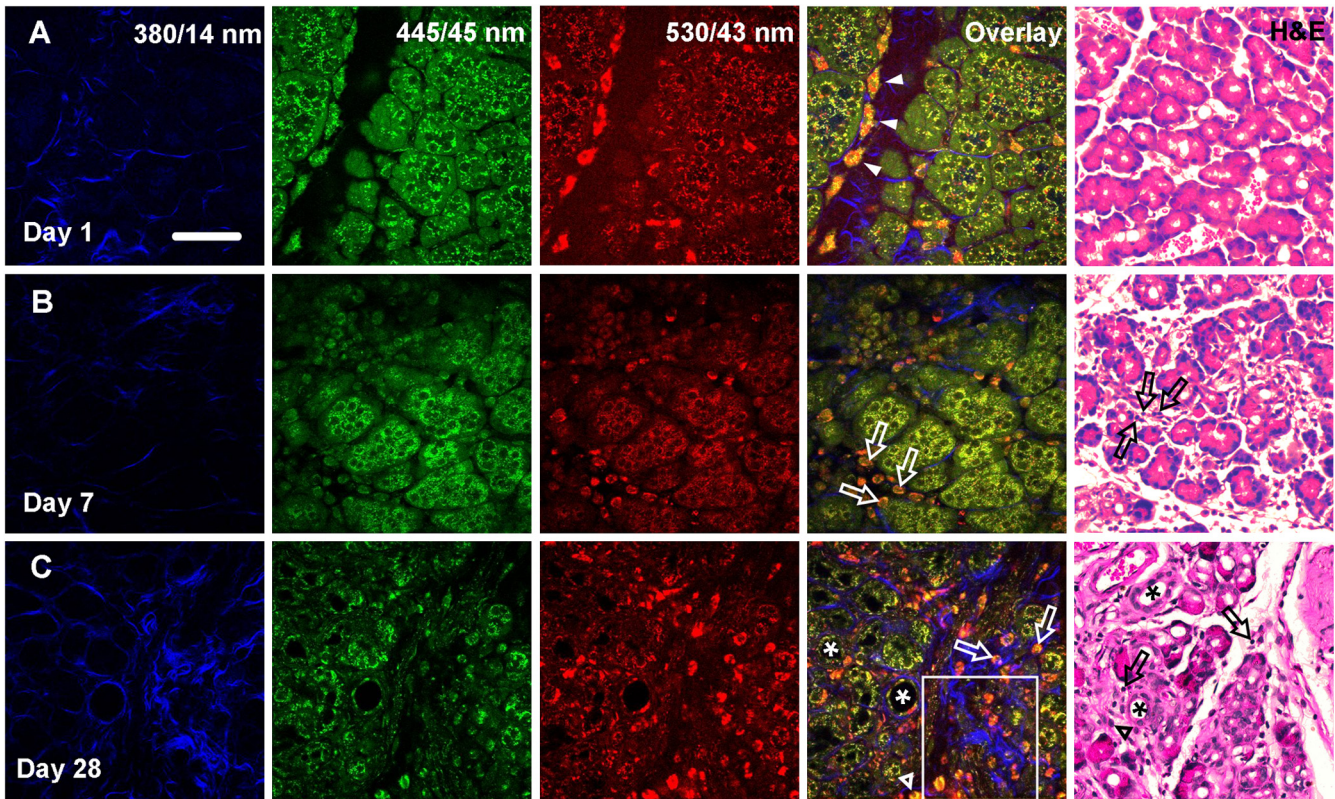


Fig. 3 Simultaneous visualization of PSCs, inflammatory infiltrates, and collagen fibers during chronic pancreatitis. (a) In the nonlinear optical images (the first four columns), the morphology of the PSCs (solid arrowheads) in the pancreatic tissues harvested one day after induction of chronic pancreatitis changed from star-like to triangular shape. (b) At day 7, the PSCs are visually absent due to the decrease of retinol fluorescence in the red channel. Lymphocytes without cellular processes (open arrows) appeared in the pancreatic tissues. Slight fibrosis can be observed. (c) A few macrophages with larger size and visible cellular inclusions (open arrowhead) can be seen in the pancreatic tissues at day 28 except for the lymphocytes (open arrows). Besides, the tubular complexes (asterisks) and intense deposition of collagen fibers indicate the progress of chronic pancreatitis. The corresponding H&E images (right column) are consistent with the above results obtained by nonlinear optical microscopy. Scale bar is 60 μm .

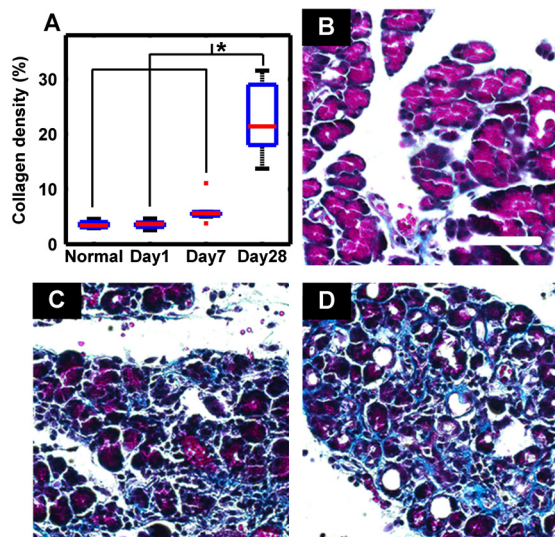


Fig. 4 Content of collagen fibers during chronic pancreatitis. (a) Quantitative analysis of the SHG images show that the density of collagen fibers in the tissues harvested at 28 days after the induction of pancreatitis is significantly larger than those of the other groups. *, $p < 0.001$, ANOVA linear contrast. The sample size is 8 for each group (eight rats); +, outliers on the box-and-whisker diagram; bars, total extent of the data. The Masson's trichrome images of pancreatic tissues at (b) day 1, (c) day 7, and (d) day 28 are in agreement with the quantitative results. Scale bar is 60 μm .

epithelium.³³ Besides, the overall pattern is the same as the vessels revealed by fluorescent agents and transgenic reporters.^{34,35} Microvessels are also observed in the other groups of pancreatic tissues (Fig. 6), and they are relatively rare in the pancreatic tissues selected. It suggests angiogenesis in the inflammatory pancreatic tissues as pancreatitis progress, which has been reported by previous studies³⁶ and can be confirmed by high vascular density in the H&E-stained image of pancreatic tissues at day 28 [Fig. 3(c)].

Based on intrinsic emission and morphology, other pancreatic components including the lymphocytes, macrophages, collagen fibers, and blood vessels can also be visualized simultaneously with the acinar cells using nonlinear optical microscopy. In particular, their corresponding alterations including inflammatory cell invasion, destruction of acinar cells, tubular complex formation, and fibrosis can be characterized simultaneously and related with different stages of chronic pancreatitis.

3.3 Phenotype Conversions of PSCs Within 3-D Tissue Structure

The changes of PSCs during chronic pancreatitis are investigated by the pancreatic tissues harvested at different stages. At day 1 after the induction of chronic pancreatitis, the PSCs exhibit shorter cellular processes and take on a triangle-shaped morphology [solid arrowheads in Fig. 3(a)]. This is in agreement with previously reported morphological transformation of PSCs

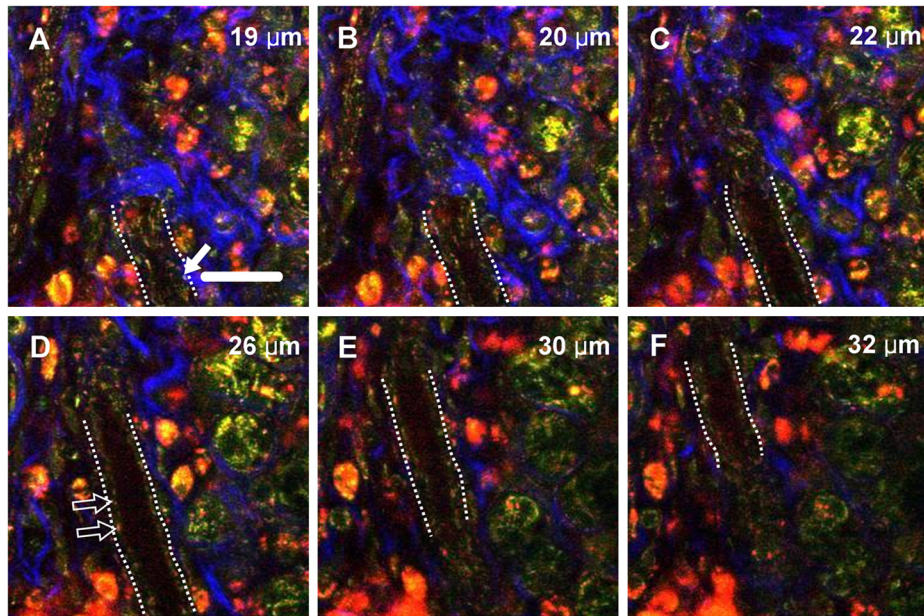


Fig. 5 Magnified images of the blood vessel acquired at different imaging depths corresponding to the area indicated by the white box in Fig. 3(c). In the pancreatic tissues at day 28 after the induction of chronic pancreatitis, blood vessels (dotted lines) are present in the inflamed area with pericytes (solid arrow) around the endothelial cells (open arrows). The imaging depths within the tissues are indicated by the z value in the upper right corner of each image. Scale bar is 30 μm .

on day 3 in a culture model.³⁷ In addition, the PSCs increase in size [Fig. 3(a)] compared with those in normal pancreas [Fig. 1(d)]. It is difficult to quantitatively assess the size of the fibroblast-like PSCs using conventional histological methods, due to the disconnections between tissue sections generally with a thickness of 4 to 7 μm . In comparison, the inherent optical sectioning ability and high spatial resolution of nonlinear optical microscopy allows accurate quantitative analysis of cell size within 3-D tissue structure. Our result shows significant enlargement of the PSCs compared with the normal group (Fig. 7;

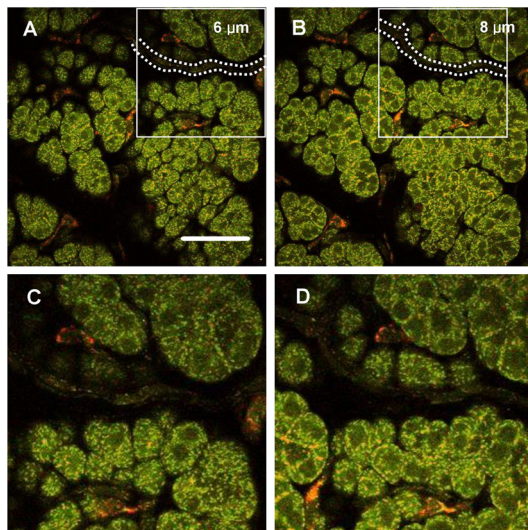


Fig. 6 Microvessel in a normal pancreas. (a) and (b) The morphology of microvessel is delineated by the dotted lines in the images acquired at various depths within the tissues as indicated by the z value in the upper right corner of each image. (c) and (d) The endothelium and the thin lumen of the microvessel can be clearly seen in the magnified images corresponding to the areas indicated by the white box in (a) and (b). Scale bar is 60 μm .

$p < 0.001$, two-tailed t test on the size of the PSCs; $n = 8$ for each group), and the area of PSCs increases by about 1.75 times from normal group to the day 1 group.

After 7 days of chronic pancreatitis, the PSCs can hardly be visualized in the inflamed area [Fig. 3(b) and 3(c)], largely due to the loss of retinol-containing fat droplets, which is related to the activation of PSCs.¹ We further verified the activation of PSCs by coexpression of desmin and α -SMA. In the corresponding immunostained images, the PSCs are seen to be quiescent on day 1 after the induction of pancreatitis [Fig. 8(a) and 8(b)], indicating the enlargement of endoplasmic reticulum network as an early event before they become activated.¹ As chronic pancreatitis progresses, the PSCs gradually convert to an activated state [Fig. 8(c)–8(f)]. Besides, the number of α -SMA-positive cells

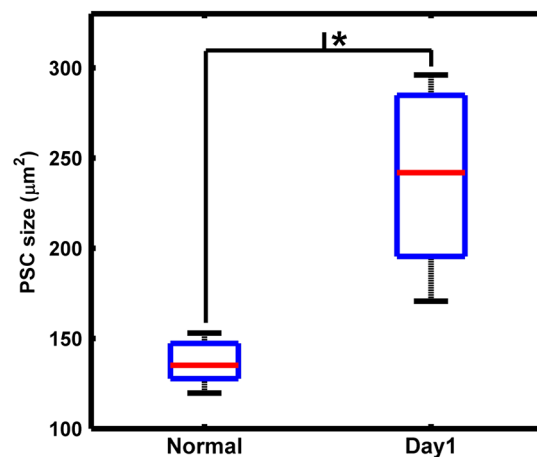


Fig. 7 Quantitative analysis of the size of the PSCs. The PSCs in the tissues harvested at day 1 after the induction of pancreatitis are significantly larger than those in the normal pancreas. *, $p < 0.001$, two-tailed t test on the size of the PSCs. The sample size is 8 for each group (eight rats). Bars, total extent of the data.

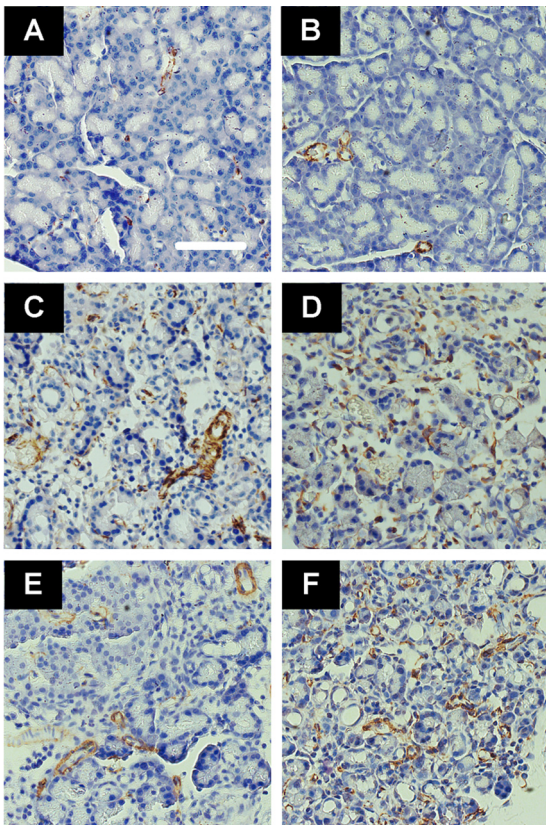


Fig. 8 Immunostaining for the assessment of PSC phenotype. The PSCs in pancreatic tissues harvested at 1 day [(a) and (b)], 7 days [(c) and (d)], and 28 days [(e) and (f)] after the induction of pancreatitis were immunostained by desmin [(a), (c), and (e)] and α -SMA [(b), (d), and (f)] expressions, which shows that the PSCs are quiescent at day 1 and they gradually transformed to an activated phenotype as chronic pancreatitis progressed. Scale bar is 60 μ m.

increased significantly from day 1 to 28 [Fig. 8(d) and 8(f)], which is possibly from a bone-marrow origin.³⁸

It can be seen from the above results that the fluorescence from vitamin A enables morphological characterization of PSCs within 3-D tissue structure before they become activated. After the loss of vitamin A in the cell, the TPEF intensity of PSCs in the red channel decreased. Because the cells are densely arranged in the pancreatic tissues, the PSCs are hard to be identified from the acinar cells according to the cell morphology revealed by NADH and FAD fluorescence. Nonetheless, loss of vitamin A fluorescence can be used as an indicator for the phenotype conversions of PSCs during chronic pancreatitis.

4 Discussion

In this study, three channels with different bandpass filters are used to collect signals from pancreatic tissues. Difference of signal intensity between these spectral windows can provide additional spectral information to distinguish cells with different intrinsic fluorophores, such as NADH, FAD, and vitamin A. The quiescent PSCs with abundant vitamin A-containing lipid droplets are recognized from the acinar cells with intracellular fluorescence mainly from NADH. The small lymphocytes with a round or oval shape are distinguished from the star-like PSCs by the morphology. They show higher fluorescence intensity in the red channel, which is consistent with the reported broad emission that probably originates from phospholipids.¹⁶ Nonlinear optical imaging has been reported to reveal the morphology of pancreatic tissues in our previous work.²⁹ However, only one detection channel was used for the collection of intracellular fluorescence primarily from NADH. This makes it hard to distinguish nonacinar cells from the acinar cells based on the morphology, due to the dense arrangement of cells in the pancreatic tissues. In the current study, we demonstrate that the combination of spectral information and morphological features

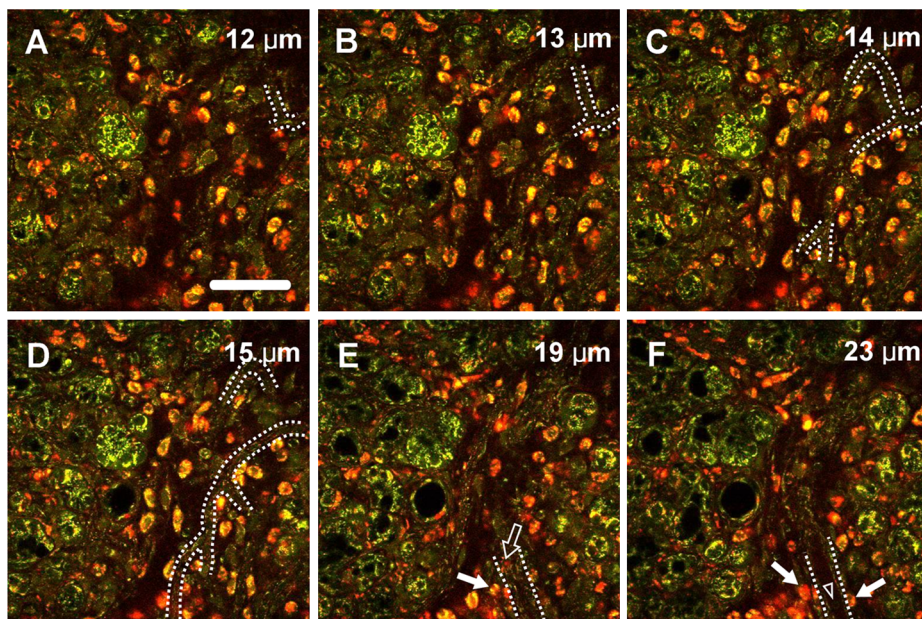


Fig. 9 Three-dimensional (3-D) morphology of the vasculature and inflammatory infiltrates within pancreatic tissues at day 28. (a)–(d) The blood vessel network (dotted lines) can be seen in the superimposed nonlinear optical images at various depths within the tissues as indicated by the z value in the upper right corner of each image. (e)–(f) The leukocytes are found near the outer vessel walls (solid arrows), close to the endothelium (open arrow), and circulating through the small blood vessels (open arrowhead). Scale bar is 60 μ m.

enables simultaneous identification of the acinar cells, PSCs, inflammatory cells, blood vessels, and collagen fibers using nonlinear optical microscopy.

Based on the multichannel detection and morphological features, the alterations of multiple pancreatic components during chronic pancreatitis are observed simultaneously within 3-D tissue environment, including the inflammatory invasion at day 7, destruction of acini and tubular complex formation at day 28, progress of fibrosis at days 7 and 28, which are similar with the reported histological findings using a DBTC-induced model.³⁹ In addition, the PSC transformation indicated by the intrinsic fluorescence and the enlargement of PSCs before activation are observed in pancreatic tissues. However, the PSCs lose vitamin A autofluorescence after activation, which limits the simultaneous visualization of PSCs and the other pancreatic components. It suggests that nonlinear optical imaging based on intrinsic optical biomarkers is more effective for the investigation of exocrine pancreatic diseases at early stages.

The lymphocytes and macrophages can be distinguished from each other in an inflamed pancreas by their morphology revealed by intrinsic fluorescence. For detailed recognition of different inflammatory cell types and investigation of individual cell behavior, a fluorescent probe or label can be introduced into cells or structures of interest.⁴⁰ We have visualized the spatial distribution of the inflammatory cells and the capillary blood vessels [dotted lines in Fig. 9(a)–9(d)] within a 3-D tissue environment at day 28. The inflammatory cell close to the endothelium [open arrow in Fig. 9(e)] and circulating leukocyte [open arrow in Fig. 9(f)] can be observed in a postcapillary venule about 20 μm in diameter. The number of inflammatory cells observed in postcapillary venules is small, probably due to the lack of lymphatic inputs and normal blood flow in freshly excised tissues.⁴¹ More in-depth time-course or intravital studies may reflect the natural dynamics of biological processes and cell–cell/matrix interactions under physiological conditions,⁴² which would facilitate dissecting the relationship between PSCs and angiogenesis, recruitment of inflammatory infiltrates, as well as fibrosis. Recently, a new technique for the *in vivo* imaging of autoimmune diabetes development in the pancreas is designed and allows for real-time visualization of interactions between cells,⁴³ which might be implemented to investigate the pathological processes during exocrine pancreatic diseases in living animals. Further translation to other exocrine pancreatic disease models such as a spontaneous pancreatic cancer model should greatly improve our understanding of the disease pathogenesis and offer more effective treatment for exocrine pancreatic diseases.

Recently, specific treatment strategies targeting PSCs have been tested, indicating potential treatments for pancreatic disorders.^{44,45} The inhibition or reversion of the PSC activation process, as well as induction of apoptosis in activated PSCs represent a promising new strategy for reducing fibrogenesis.¹ Vitamin A and its metabolites all-trans retinoic acid and 9-cis retinoic acid have been reported to inhibit PSC activation.⁴⁴ In our study, the fluorescence of vitamin A can be detected by nonlinear optical microscopy as an indicator for the phenotype of PSCs. As a result, further application of this technique to the study of PSC targeting might be of benefit for the development of therapeutic strategies.

Acknowledgments

We would like to thank Xiaobao Liang and Hui Li for their help with spectral measurements and quantitative analysis,

respectively. We greatly appreciate Chunyou Wang and Gang Zhao from Union Hospital at Huazhong University of Science and Technology for their suggestions. The authors also thank the Analytical and Testing Center (Huazhong University of Science and Technology) for spectral measurements. This work was supported by the National Major Scientific Research Program of China (No. 2011CB910401), National Natural Science Foundation of China (No. 61178077), National Key Technology R&D Program of China (No. 2011BAI12B06), and Wuhan Youth Science and Technology Program (No. 201271031424).

References

1. M. B. Omary et al., "The pancreatic stellate cell: a star on the rise in pancreatic diseases," *J. Clin. Invest.* **117**(1), 50–59 (2007).
2. P. Mews et al., "Pancreatic stellate cells respond to inflammatory cytokines: potential role in chronic pancreatitis," *Gut* **50**(4), 535–541 (2002).
3. M. Hidalgo, "Pancreatic cancer," *N. Engl. J. Med.* **362**(17), 1605–1617 (2010).
4. B. Farrow, D. Albo, and D. H. Berger, "The role of the tumor micro-environment in the progression of pancreatic cancer," *J. Surg. Res.* **149**(2), 319–328 (2008).
5. H. Schmitz-Winnenthal et al., "Chronic pancreatitis is associated with disease-specific regulatory T-cell responses," *Gastroenterology* **138**(3), 1178–1188 (2010).
6. A. Masamune et al., "Roles of pancreatic stellate cells in pancreatic inflammation and fibrosis," *Clin. Gastroenterol. Hepatol.* **7**(11), S48–S54 (2009).
7. A. Masamune et al., "Hypoxia stimulates pancreatic stellate cells to induce fibrosis and angiogenesis in pancreatic cancer," *Am. J. Physiol. Gastrointest. Liver Physiol.* **295**(4), G709–G717 (2008).
8. A. Casini et al., "Collagen type I synthesized by pancreatic peri-acinar stellate cells (PSC) co-localizes with lipid peroxidation-derived aldehydes in chronic alcoholic pancreatitis," *J. Pathol.* **192**(1), 81–89 (2000).
9. B. A. Neuschwander-Tetri et al., "Repetitive acute pancreatic injury in the mouse induces procollagen alpha(1)(I) expression colocalized to pancreatic stellate cells," *Lab. Invest.* **80**(2), 143–150 (2000).
10. A. Kuno et al., "Angiotensin-converting enzyme inhibitor attenuates pancreatic inflammation and fibrosis in male Wistar Bonn/Kobori rats," *Gastroenterology* **124**(4), 1010–1019 (2003).
11. H. Algful et al., "Mechanisms of disease: chronic inflammation and cancer in the pancreas—A potential role for pancreatic stellate cells?," *Nat. Clin. Pract. Gastroenterol. Hepatol.* **4**(8), 454–462 (2007).
12. M. G. Bachem et al., "Role of stellate cells in pancreatic fibrogenesis associated with acute and chronic pancreatitis," *J. Gastroenterol. Hepatol.* **21**(Suppl. 3), S92–S96 (2006).
13. M. V. Apte et al., "Periacinar stellate shaped cells in rat pancreas: identification, isolation, and culture," *Gut* **43**(1), 128–133 (1998).
14. M. Erkan et al., "StellaTUM: current consensus and discussion on pancreatic stellate cell research," *Gut* **61**(2), 172–178 (2012).
15. S. J. Pandol, "Are we studying the correct state of the stellate cell to elucidate mechanisms of chronic pancreatitis?," *Gut* **54**(6), 744–745 (2005).
16. L. E. Grosberg et al., "Spectral characterization and unmixing of intrinsic contrast in intact normal and diseased gastric tissues using hyperspectral two-photon microscopy," *PLoS One* **6**(5), e19925 (2011).
17. Y. Y. Fu et al., "Three-dimensional optical method for integrated visualization of mouse islet microstructure and vascular network with sub-cellular-level resolution," *J. Biomed. Opt.* **15**(4), 046018 (2010).
18. F. Helmchen and W. Denk, "Deep tissue two-photon microscopy," *Nat. Meth.* **2**(12), 932–940 (2005).
19. W. R. Zipfel, R. M. Williams, and W. W. Webb, "Nonlinear magic: multiphoton microscopy in the biosciences," *Nat. Biotechnol.* **21**(11), 1369–1377 (2003).
20. A. Zoumi, A. Yeh, and B. J. Tromberg, "Imaging cells and extracellular matrix *in vivo* by using second-harmonic generation and two-photon excited fluorescence," *Proc. Natl. Acad. Sci. U. S. A.* **99**(17), 11014–11019 (2002).

21. W. R. Zipfel et al., "Live tissue intrinsic emission microscopy using multiphoton-excited native fluorescence and second harmonic generation," *Proc. Natl. Acad. Sci. U. S. A.* **100**(12), 7075–7080 (2003).
22. P. Steven et al., "Experimental induction and three-dimensional two-photon imaging of conjunctiva-associated lymphoid tissue," *Investig. Ophthalmol. Vis. Sci.* **49**(4), 1512–1517 (2008).
23. J. N. Rogart et al., "Multiphoton imaging can be used for microscopic examination of intact human gastrointestinal mucosa ex vivo," *Clin. Gastroenterol. Hepatol.* **6**(1), 95–101 (2008).
24. N. D. Kirkpatrick, M. A. Brewer, and U. Utzinger, "Endogenous optical biomarkers of ovarian cancer evaluated with multiphoton microscopy," *Cancer Epidemiol. Biomarkers Prevention* **16**(10), 2048–2057 (2007).
25. M. C. Skala et al., "Multiphoton microscopy of endogenous fluorescence differentiates normal, precancerous, and cancerous squamous epithelial tissues," *Cancer Res.* **65**(4), 1180–1186 (2005).
26. O. D. Smirnova, D. A. Rogatkin, and K. S. Litvinova, "Collagen as in vivo quantitative fluorescent biomarkers of abnormal tissue changes," *J. Innov. Opt. Health Sci.* **5**(2), 1250010 (2012).
27. J. V. Rocheleau et al., "Pancreatic islet beta-cells transiently metabolize pyruvate," *J. Biol. Chem.* **277**(34), 30914–30920 (2002).
28. J. V. Rocheleau, W. S. Head, and D. W. Piston, "Quantitative NAD(P)H/ flavoprotein autofluorescence imaging reveals metabolic mechanisms of pancreatic islet pyruvate response," *J. Biol. Chem.* **279**(30), 31780–31787 (2004).
29. W. Hu et al., "Nonlinear optical microscopy for histology of fresh normal and cancerous pancreatic tissues," *PLoS One* **7**(5), e37962 (2012).
30. J. H. Won et al., "Phenotypic changes in mouse pancreatic stellate cell Ca²⁺ signaling events following activation in culture and in a disease model of pancreatitis," *Mol. Biol. Cell.* **22**(3), 421–436 (2011).
31. H. F. Zhao et al., "Anti-monocyte chemoattractant protein 1 gene therapy attenuates experimental chronic pancreatitis induced by dibutyltin dichloride in rats," *Gut* **54**(12), 1759–1767 (2005).
32. C. Bayan et al., "Fully automated, quantitative, noninvasive assessment of collagen fiber content and organization in thick collagen gels," *J. Appl. Phys.* **105**(10), 102042 (2009).
33. W. J. Clif, *Blood Vessels*, Cambridge University Press, Cambridge (1976).
34. J. D. Lewis et al., "Viral nanoparticles as tools for intravital vascular imaging," *Nat. Med.* **12**(3), 354–360 (2006).
35. F. Hillen et al., "A transgenic Tie2-GFP athymic mouse model; a tool for vascular biology in xenograft tumors," *Biochem. Biophys. Res. Commun.* **368**(2), 364–367 (2008).
36. R. Kuehn et al., "Angiogenesis, angiogenic growth factors, and cell adhesion molecules are upregulated in chronic pancreatic diseases: angiogenesis in chronic pancreatitis and in pancreatic cancer," *Pancreas* **18**(1), 96–103 (1999).
37. F. Manapov, P. Muller, and J. Rychly, "Translocation of p21(Cip1/WAF1) from the nucleus to the cytoplasm correlates with pancreatic myofibroblast to fibroblast cell conversion," *Gut* **54**(6), 814–822 (2005).
38. G. Sparmann et al., "Bone marrow-derived pancreatic stellate cells in rats," *Cell Res.* **20**(3), 288–298 (2010).
39. M. Inoue et al., "The role of monocyte chemoattractant protein-1 in experimental chronic pancreatitis model induced by dibutyltin dichloride in rats," *Pancreas* **25**(4), e64–e70 (2002).
40. M. D. Cahalan and I. Parker, "Choreography of cell motility and interaction dynamics imaged by two-photon microscopy in lymphoid organs," *Ann. Rev. Immunol.* **26**, 585–626 (2008).
41. M. D. Cahalan et al., "Real-time imaging of lymphocytes in vivo," *Curr. Opin. Immunol.* **15**(4), 372–377 (2003).
42. M. J. Pittet and R. Weissleder, "Intravital imaging," *Cell* **147**(5), 983–991 (2011).
43. K. Coppieters et al., "A novel technique for the in vivo imaging of autoimmune diabetes development in the pancreas by two-photon microscopy," *PLoS One* **5**(12), e15732 (2010).
44. J. A. McCarroll et al., "Vitamin A inhibits pancreatic stellate cell activation: implications for treatment of pancreatic fibrosis," *Gut* **55**(1), 79–89 (2006).
45. F. E. M. Froeling et al., "Retinoic acid-induced pancreatic stellate cell quiescence reduces paracrine Wnt- β -catenin signaling to slow tumor progression," *Gastroenterology* **141**(4), 1486–1497 (2011).